MITSUBISHI ELECTRIC RESEARCH LABORATORIES
http://www.merl.com

Model-Based Condition Monitoring for Lithium-ion Batteries

Kim, T.; Wang, Y.; Sahinoglu, Z.; Wada, T.; Hara, S.; Qiao, W.

TR2015-055 November 2015

Abstract

Condition monitoring for batteries involves tracking changes in physical parameters and operational states such as state of health (SOH) and state of charge (SOC), and is fundamentally important for building high-performance and safety-critical battery systems. A model-based condition monitoring strategy is developed in this paper for Lithium-ion batteries on the basis of an electrical circuit model incorporating hysteresis effect. It systematically integrates 1) a fast upper-triangular and diagonal recursive least squares algorithm for parameter identification of the battery model, 2) a smooth variable structure filter for the SOC estimation, and 3) a recursive total least squares algorithm for estimating the maximum capacity, which indicates the SOH. The proposed solution enjoys advantages including high accuracy, low computational cost, and simple implementation, and therefore is suitable for deployment and use in real-time embedded battery management systems (BMSs). Simulations and experiments validate effectiveness of the proposed strategy.

Journal of Power Sources

This work may not be copied or reproduced in whole or in part for any commercial purpose. Permission to copy in whole or in part without payment of fee is granted for nonprofit educational and research purposes provided that all such whole or partial copies include the following: a notice that such copying is by permission of Mitsubishi Electric Research Laboratories, Inc.; an acknowledgment of the authors and individual contributions to the work; and all applicable portions of the copyright notice. Copying, reproduction, or republishing for any other purpose shall require a license with payment of fee to Mitsubishi Electric Research Laboratories, Inc. All rights reserved.

Copyright © Mitsubishi Electric Research Laboratories, Inc., 2015
201 Broadway, Cambridge, Massachusetts 02139

Model-Based Condition Monitoring for Lithium-ion Batteries ☆

Taesic Kim[a], Yebin Wang[b], Huazhen Fang[c], Zafer Sahinoglu[b], Toshihiro Wada[d], Satoshi Hara[d], Wei Qiao[e]

[a]*Department of Computer Science and Computer Engineering, University of Nebraska-Lincoln, Lincoln, NE 68588-0511 USA*
[b]*Mitsubishi Electric Research Laboratories, 201 Broadway, Cambridge, MA 02139, USA*
[c]*Department of Mechanical Engineering, University of Kansas, Lawrence, KS 66045, USA*
[d]*Advanced Technology R&D Center, Mitsubishi Electric Corporation, 8-1-1, Tsukaguchi-honmachi, Amagasaki City, 661-8661, Japan*
[e]*Department of Electrical and Computer Engineering, University of Nebraska-Lincoln, Lincoln, NE 68588-0511 USA*

Abstract

Condition monitoring for batteries involves tracking changes in physical parameters and operational states such as state of health (SOH) and state of charge (SOC), and is fundamentally important for building high-performance and safety-critical battery systems. A model-based condition monitoring strategy is developed in this paper for Lithium-ion batteries on the basis of an electrical circuit model incorporating hysteresis effect. It systematically integrates 1) a fast upper-triangular and diagonal recursive least squares algorithm for parameter identification of the battery model, 2) a smooth variable structure filter for the SOC estimation, and 3) a recursive total least squares algorithm for estimating the maximum capacity, which indicates the SOH. The proposed solution enjoys advantages including high accuracy, low computational cost, and simple implementation, and therefore is suitable for deployment and use in real-time embedded battery management systems (BMSs). Simulations and experiments validate effectiveness of the proposed strategy.

Keywords: Lithium-ion battery monitoring, fast upper-triangular and diagonal recursive least squares, maximum capacity estimation, recursive total least squares, smooth variable structure filter, state of charge, state of health

1. Introduction

Lithium-ion (Li-ion) batteries have gained widespread use in applications ranging from consumer electronics devices to power tools and to electric vehicles (EVs) due to their high energy and power densities and long cycle life [1]. However, effective battery monitoring and control, equivalently battery management systems (BMSs), remains a remarkable challenge and necessity, having spurred a wealth of research on their core algorithms [2]. A key mission of a BMS is to

☆Corresponding author Y. Wang. Tel: 001-617-621-7500; fax: 001-617-621-7550. Email address: yebinwang@ieee.org

monitor the state of charge (SOC) [3, Sec. 3.2], state of health (SOH), and battery parameters including impedance and capacity [4]. A precise understanding of these variables is crucial for a series of BMS tasks, e.g., charging, discharging, cell balancing, and fault prognosis and diagnostics, to improve operational performance, safety, reliability and lifespan of batteries. However, it cannot be obtained by direct measurement and instead, needs to be built upon estimation. Such estimation algorithms are expected to have low complexity and high computational efficiency, a prerequisite for their online implementation on resource constrained platforms such as embedded BMSs.

Research efforts on online battery parameter estimation have led to two families of methods: Kalman filter (KF)-based and regression-based. A variety of KFs, including the linear KF [5], extended KF (EKF) [3], and sigma point KF (SPKF) [6] have been used to estimate battery parameters and states simultaneously. Compared to the KF-based solution, the least squares method and its variant are more computationally competitive without compromising much accuracy, thus holding significant potential for battery model identification. See [7–11] and references therein for details. Recently, an upper-triangular and diagonal (UD) factorization-based RLS estimation method with an EF [12] was proposed to solve the digital computer implementation problem of the RLS. In additional to fast speed, this method has improved numerical stability with preservation of a positive covariance.

The SOC estimation has been a subject of intensive research, which leads to a variety of estimation algorithms. The easiest-to-implement ones include voltage translation and Coulomb counting [13]. However, multiple issues render them unreliable, especially the sensitivity to initial SOC estimate and accumulative integration errors. The computational intelligence (CI)-based methods, e.g., artificial neural network (ANN) [14], fuzzy logic [15], and support vector machine [16], conduct the SOC estimation through data-driven learning of the nonlinear relationship between the SOC and measured quantities such as battery voltage, current and temperature. The learning process is nonetheless adverse to real-time execution due to the high computational burden. Applying state filters and observers to electrochemical or electrical circuit models, model-based methods have been attracting considerable attention as an effective means to improve the SOC estimation accuracy. The EKF has been widely used for SOC estimation [17, 18], and its upgraded variant, the iterated EKF (IEKF), is used in [19] for simultaneous SOC and model parameter estimation. In [6, 20], the hysteresis effect inherent in batteries [21] is accounted for with the development of approaches based on a dual EKF and a dual sigma-point KF (SPKF), respectively. However, the IEKF, dual EKF and SPKF increases the accuracy at the expense of higher computational effort. One major alternative thus is the more computationally efficient observer-based approaches, e.g., linear observer [10], sliding mode observer [9, 11], nonlinear geometric adaptive observer [22], and partial differential equation (PDE) observer [23]. A further advantage they have is the availability of convergence analysis for the estimation error dynamics. Meanwhile, some work attempts to combine the advantages of the aforementioned methods, an example of which is the SOC estimation using neural networks and EKF in [24].

The SOH measures the battery aging and wear, which correspond to capacity fade and power fade [20]. Accordingly, battery maximum capacity [17, 25], and impedance components (e.g. impedance [26], internal resistance [27], diffusion resistance [28] and a diffusion capacitance [29]) are the commonly used parameters to quantify the SOH. Some straightforward ways to infer

SOH, e.g., evaluating the maximum capacity via a full discharge test with a small current [25] or measuring the impedance [26], are not suitable for real-time estimation. This is because the maximum capacity declines gradually due to the aging and degradation, and fluctuates according to temperature. A knowledge of its accurate value is indispensable for SOC estimation (especially in the standalone case), health prognosis and other battery management tasks. The online SOH estimation has been tackled by CI-based methods, e.g., ANN [30, 31], adaptive recurrent NN [32], and structured neural network (SNN) [33], and model-based methods, such as the dual EKF [6, 17, 20, 34] and the dual sliding mode observer [35]. Additionally, analytical approaches, including the two-point (TP) of SOCs method [11] and recursive total least squares (RTLS) [36], have been developed and exploited to estimate the maximum capacity based on Coulomb counting.

This paper proposes a comprehensive strategy for online condition monitoring of Li-ion batteries. Its design is based on a battery model that captures both the electrical circuit characteristics and the hysteresis. The monitoring solution consists of three interrelated algorithms for battery parameter, SOC, and SOH estimation, respectively. Specifically, a fast UD recursive least squares (FUDRLS) method is built to identify the battery model parameters. Based on the fully identified model, a smooth variable structure filter (SVSF) is designed to perform the SOC estimation. Finally, the battery's maximum capacity is determined by a Rayleigh quotient-based RTLS algorithm taking the estimated SOCs and measured current as inputs. The proposed algorithms are integrated to run in parallel but at multiple time scales to achieve the best use of computational resources. A short time scale is used in FUDRLS and SVSF to deal with the fast time-varying electrical parameters and SOC, and the RTLS algorithm is executed at a longer time scale for tracking the slowly time-varying capacity. The proposed strategy is endowed with high computational efficiency and accuracy, and thus is suitable for real-time embedded BMS applications. The proposed method is validated by both simulation and experimental studies.

2. The Real-time Battery Model

The battery model should be carefully chosen to ensure high-quality state and parameter estimation. In particular, a balance between the fidelity and complexity of the battery model should be made for the real-time condition monitoring in embedded BMSs. Electrical circuit battery models are arguably the most suitable for embedded applications due to their low complexity and the ability of characterizing the current-voltage dynamics of battery cells [37]. A real-time electric circuit model with the hysteresis will be considered throughout the paper. The voltage hysteresis effect between the charge and discharge curve widely exists in Li-ion batteries, especially the popular $LiFePO_4$-type [21]. The SOC estimation accuracy will deteriorate if the battery model fails to account for this phenomenon. The model considered here is based on a first-order RC electrical circuit with hysteresis, as shown in Fig. 1, which features both simplicity and effectiveness [38].

As shown in Fig. 1, the open-circuit voltage (OCV), denoted as V_{oc}, includes two parts. The first part, $V_s(SOC)$, represents the average equilibrium OCV as a function of the SOC. Since the V_s is bijective, the SOC can be inferred from V_s. The second part V_h is the hysteresis voltage to capture the hysteresis behavior of the OCV curves. The RC circuit models the current-voltage characteristics and the transient response of the battery cell. Particularly, the series resistance, R_s, is used to describe the charge/discharge energy loss in the cell; the charge transfer resistance,

R_c, and double layer capacitance, C_d, are used to characterize the charge transfer and short-term diffusion voltage, V_d, of the cell; V_B represents the terminal voltage of the cell.

Fig. 2 shows two measured OCV curves and their average: $V_{oc,c}$, $V_{oc,d}$, and $V_{oc,a}$, respectively. Particularly, $V_{oc,c}$ and $V_{oc,d}$ are obtained by slowly charging and discharging the battery, and represent major upper and lower hysteresis loops, respectively. We treat the average voltage $V_{oc,a}$ as $V_s(SOC)$. The instantaneous open circuit voltage V_{oc} is bounded by the major hysteresis loops. By subtracting $V_h(k)$ from V_{OC}, the $V_s(SOC)$ can be extracted.

We will use the following voltage hysteresis model [39]:

$$\frac{\partial V_h}{\partial t} = -\rho(\eta i_B - \upsilon S_D)[V_{h\max} + \text{sign}(i_B)V_h], \tag{1}$$

where ρ is the hysteresis parameter representing the convergence rate, η the Coulomb efficiency (assuming $\eta = 1$), i_B the instantaneous current applied to the battery, υ the self-discharge multiplier for hysteresis expression, S_D the self-discharge rate, and $V_{h\max}$ the maximum hysteresis voltage. The model (1) describes the dependency of the hysteresis voltage V_h on the current, self-discharge, and hysteresis boundaries. The parameter ρ is chosen to minimize the voltage error between the $V_{oc} - SOC$ curves from simulation and experiments, respectively. Note that ρ and $V_{h\max}$ may depend on the SOC and the battery temperature [21, 39].

A discrete-time battery model, including the electrical circuit model and the hysteresis model, can be written as follows

$$\begin{aligned} X(k+1) &= \begin{bmatrix} 1 & 0 & 0 \\ 0 & \gamma & 0 \\ 0 & 0 & H \end{bmatrix} X(k) + \begin{bmatrix} -\frac{\eta T_s}{C_{\max}} & 0 \\ R_c(1-\gamma) & 0 \\ 0 & (H-1)\text{sign}(i_B) \end{bmatrix} \begin{bmatrix} i_B(k) \\ V_{h\max} \end{bmatrix}, \\ y(k) &= V_B(k) = V_{oc}(SOC(k)) - V_d(k) - R_s i_B(k) + V_h(k), \\ V_s(SOC) &= a_0 \exp(-a_1 SOC) + a_2 + a_3 SOC - a_4 SOC^2 + a_5 SOC^3, \end{aligned} \tag{2}$$

where $X(k+1) = \begin{bmatrix} SOC(k+1) & V_d(k+1) & V_h(k+1) \end{bmatrix}^T$ is the state, $y(k)$ is the measured output, k is the time index, $C_{\max}$ denotes the maximum capacity of the battery, T_s is the sampling period, $\gamma = \exp(\frac{-T_s}{\tau})$ with $\tau = R_c C_d$, $H(i_B) = \exp(-\rho |i_B| T_s)$, and a_j for $0 \le j \le 5$ are the coefficients used to parameterize the V_{oc}-SOC curve. A concise form of the dynamics (2) is given by

$$\begin{aligned} X(k+1) &= f(X(k), i_B(k)), \\ y(k) &= h(X(k), i_B(k)), \end{aligned}$$

where f and h are vectors of smooth functions with appropriate dimensions. Coefficients a_j for $0 \le j \le 5$ can be extracted by pulsed current tests [37] or constant charge and discharge current test using a small current to minimally excite transient response of the battery cell [40]. Although the temperature dependency is ignored in this paper by testing the battery under the ambient temperature, the proposed strategy might be extended to incorporate the thermal effects.

3. The Proposed Strategy

The proposed condition monitoring strategy, shown in Fig. 3, consists of three parts:

1) an FUDRLS-based parameter estimator,
2) an SVSF-based SOC estimator, and
3) an RTLS-based SOH (i.e., capacity) estimator.

The strategy operates at different time scales, where the FUDRLS and SVSF runs at a fast speed to estimate the fast time-varying parameters and the SOC, and the RTLS runs slower to track the slowly time-varying capacity parameter. In this way will the computational resources be used economically with guaranteed estimation performance.

3.1. Parameter Estimation by the FUDRLS

Since battery parameters (e.g, impedance) change with the SOC, temperature, and current rates, etc., online parameter estimation is required. Previous work [41] formulated the impedance estimation as a least squares (LS) problem and proposed the FUDRLS algorithm to identify three impedance parameters: R_s, R_c, and C_d. In this paper, we overcome the difficulty due to the time-varying dynamics and establish that both the impedance and the hysteresis parameter estimation can be approximately formulated as an LS problem, and thus the FUDRLS can be readily employed to estimate the hysteresis parameter $V_{h\max}$.

We first present procedures for impedance estimation for completeness, then show how similar idea can be used to estimate the hysteresis parameter. To estimate the impedance, we ignore the hysteresis voltage dynamics, and assume $V_{oc} = b_1 SOC + b_0$. The battery model (2) is reduced to

$$\begin{aligned} \begin{bmatrix} SOC(k+1) \\ V_d(k+1) \end{bmatrix} &= A \begin{bmatrix} SOC(k) \\ V_d(k) \end{bmatrix} + Bi_B(k), \\ V_B(k) &= C \begin{bmatrix} SOC(k) \\ V_d(k) \end{bmatrix} + Di_B(k) + b_0, \end{aligned} \tag{3}$$

where

$$A = \begin{bmatrix} 1 & 0 \\ 0 & \gamma \end{bmatrix}, \quad B = \begin{bmatrix} \frac{-\eta T_s}{C_{\max}} \\ R_c(1-\gamma) \end{bmatrix}, \quad C = \begin{bmatrix} b_1 & -1 \end{bmatrix}, \quad D = -R_s.$$

Taking z-transformation of (3), we have [42]

$$\frac{\bar{V}_B(z)}{i_B(z)} = C(zI_2 - A)^{-1}B + D = \frac{x_3 + x_4 z^{-1} + x_5 z^{-2}}{1 + x_1 z^{-1} + x_2 z^{-2}}, \tag{4}$$

where $\bar{V}_B(z) = V_B(z) - b_0$, $I_2 \in \mathbb{R}^{2\times 2}$ is an identity matrix, and

$$\begin{aligned} x_1 &= \gamma - 1, \quad x_2 = \gamma, \quad x_3 = -R_s, \\ x_4 &= \frac{-b_1 T_s}{C_{\max}} + R_c(\gamma - 1) + R_s(\gamma + 1), \\ x_5 &= R_c(1-\gamma) + \gamma\left(\frac{b_1 T_s}{C_{\max}} - R_s\right). \end{aligned}$$

The difference equation corresponding to (4) is given by

$$V_B(k) = -x_1 V_B(k-1) - x_2 V_B(k-2) + x_3 i_B(k) + x_4 i_B(k-1) + x_5 i_B(k-2) + b_0(1+x_1+x_2). \quad (5)$$

Considering $1+x_1+x_2 = 0$, (5) can be reformulated into the following regression form

$$V_B(k) - V_B(k-1) = \Phi^T(k)\Theta, \quad (6)$$

where $\Theta = [x_2, x_3, x_4, x_5]^T$, and

$$\Phi^T(k) = \begin{bmatrix} V_B(k-1) - V_B(k-2) & i_B(k) & i_B(k-1) & i_B(k-2) \end{bmatrix}.$$

Since the map from parameters R_s, R_c, C_d and b_1 to Θ is a diffeomorphism, one can uniquely determine the estimates of parameters R_s, R_c, C_d, b_1 from the estimated Θ.

Remark 1. *The approach proposed above leads to a regression model for impedance estimation. It does not require additional high-pass filtering [8], thus saving on computational cost and additional effort to develop a high-pass filter. Moreover, it brings better accuracy than the methods assuming a constant V_{oc} [7, 9, 12], especially when V_{oc} is highly nonlinear with respect to the SOC. In addition, the form given in* (6) *only uses four parameters while the work [10, 11] utilizes five parameters.*

Remark 2. *Because matrices A, B, C, D are time invariant, the z-transformation technique is applicable to derive* (6)*. Alternatively, one can perform derivation in the time domain, i.e., directly work on the difference equation* (5)*, and establish* (6)*.*

The derivation of (6) is performed on the basis of the second-order battery model (3) and parameterizing V_{oc} as $b_0 + b_1 SOC$. Specifically, linear parameterizations of the V_{oc} is critical to the derivation, and the second-order battery model (6) is merely to simplify the presentation. Linear parameterizations of V_{oc} is valid in a neighborhood of *SOC* while the hysteresis voltage $v_{h\max}$ reaches steady state, but is invalid during the transient of V_h. We propose to address this limitation by imposing a less restrictive assumption: linear parameterizations of the V_s-SOC curve, which is always valid locally. This allows us to perform parameter identification based on the following dynamics

$$\begin{aligned} X(k+1) &= \begin{bmatrix} 1 & 0 & 0 \\ 0 & \gamma & 0 \\ 0 & 0 & H \end{bmatrix} X(k) + \begin{bmatrix} -\frac{\eta T_s}{C_{\max}} & 0 \\ R_c(1-\gamma) & 0 \\ 0 & (H-1)\mathrm{sign}(i_B) \end{bmatrix} \begin{bmatrix} i_B(k) \\ V_{h\max} \end{bmatrix}, \\ y(k) &= b_0 + b_1 SOC - V_d(k) - R_s i_B(k) + V_h(k). \end{aligned} \quad (7)$$

Note that notation b_0, b_1 are abused here.

Since the state matrices are current-dependent or time-varying, the model (7) does not admit $z-$transformation. It is not straightforward to rewrite (7) into a linear regression form. We however show that an approximate linear regression form of the model (7) can be derived, and thus

parameter identification can be readily carried out. Notice that the main difficulty in establishing the linear regression form arises from the time-varying V_h-dynamics, which is fortunately independent of the V_d and SOC-dynamics. This decoupling feature allows us to obtain an approximate linear regression form.

We essentially try to obtain an approximate linear parameterization of y. We consider the following system

$$\xi(k+1) = H\xi(k) + (H-1)\text{sign}(i_B), \quad \xi(0) = \xi_0.$$

Considering $V_h(k) = \xi(k)V_{h\max}$ for $\xi_0 = V_h(0)/V_{h\max}$, we obtain linear parameterizations of $y(k)$ as follows

$$y(k) = b_0 + b_1 SOC(k) - V_d(k) - R_s i_B(k) + \xi(k)V_{h\max}, \tag{8}$$

where $V_{h\max}$ is unknown. We introduce a time-varying open-loop filter to estimate ξ

$$\hat{\xi}(k+1) = H\hat{\xi}(k) + (H-1)\text{sign}(i_B), \quad \hat{\xi}(0) = 0.$$

Since $H < 1$, the aforementioned time-varying open-loop filter produces an exponentially convergent estimate of $\xi(k)$, i.e., $\hat{\xi}(k)$ converges to $\xi(k)$ as $k \to \infty$ for any bounded ξ_0. Combining (9) and the fact that $\hat{\xi}(k) \to \xi(k)$ as $k \to \infty$, we have the approximate linear parameterizations of $y(k)$ as follows

$$y(k) = b_0 + b_1 SOC(k) - V_d(k) - R_s i_B(k) + \hat{\xi}(k)V_{h\max}, \tag{9}$$

from which, together with dynamics of SOC, V_d, the approximate linear regression of (7) can be established. Compared to (6), the approximate linear regression has an extra parameter $V_{h\max}$ in Θ, and an extra signal $\hat{\xi}(k)$ in $\Phi(k)$.

Given (6), the parameter vector Θ can be estimated by a multitude of algorithms, for instance the conventional Bierman's UD method [12], Gentleman's UDRLS [43], etc. The Gentleman's UDRLS is attractive to embedded applications due to its parallel implementation and the resultant fast computational speed. The RLS-based methods can be improved by using the forgetting factor [7]. The estimation algorithm with a small forgetting factor may track time-varying parameters fairly well at the expense of increased susceptibility to the noise; while the forgetting factor is large, the tracking ability will be poor but robust to noises. In general, the RLS technique utilizes an exponential forgetting (EF) whose forgetting rate is constant [7], [12]. The main drawback of the EF method is called wind-up, and it comes when a data vector is not persistently exciting [44] as well as non-optimal tracking ability and noise influence due to the constant forgetting rate [44].

The FUDRLS algorithm combines the Gentleman's UDRLS with a variable forgetting factor to estimate Θ. Methods with variable forgetting (VF) adaptively change the forgetting rate. The main VF mechanism is: the algorithm takes a smaller forgetting factor at the presence of large prediction errors, and a larger forgetting factor, otherwise. In this paper, the forgetting factor λ is adjusted as follows

$$\begin{aligned} \lambda(k+1) &= 1 - \frac{v_1(k)}{N_0\sigma_0^2}, \quad \lambda_{\min} \le \lambda \le \lambda_{\max}, \\ v_1(k+1) &= \delta_1 v_1(k) + (1-\delta_1)e^2(k), \end{aligned} \tag{10}$$

where δ_1 is a weighting factor to be taken close to 1; v_1 is time-average expressions of $e^2(k)$ and

$v_1(0)$ is set to be σ_0^2; the parameter σ_0^2 is the mean value of the prediction error variance obtained from the method implemented in the FUDRLS with constant forgetting factor (e.g., $\lambda = 0.98$), assuming that the expected noise variance is much smaller than σ_0^2; N_0 represents the memory length (e.g., $N_0 = 50$ corresponding to mean forgetting factor of 0.98); $\lambda_{\max}$ (e.g., 0.999) and $\lambda_{\min}$ (e.g., 0.95) denote maximum and minimum forgetting factors, respectively. An intuitive interpretation of (10) is that the forgetting factor λ is adjusted according to the square of the time-averaged estimation of the autocorrelation of posterior error $e(k)$.

In the FUDRLS, the regression matrix $\Phi^T(k)$ is combined with $v(k) = V_B(k) - V_B(k-1)$ to produce an augmented matrix:

$$\Phi_a^T(k) = \begin{bmatrix} \Phi^T(k) & v(k) \end{bmatrix}.$$

The detailed FUDRLS algorithm is given in Table 1, where δ denotes an initial covariance value (e.g., 10^5). For real-time implementation, the computation of F and the triangularization can be pipelined.

In practical BMS applications, the parameter identification algorithm can be implemented in system-on-a-chip [45]. Due to the advent of the VLSI technology, the features of parallel processing and pipelining implementation will be attractive to improve the computation speed and reduce the size of ICs [46]. The FUDRLS will be beneficial to the development of real BMS ICs in this sense.

3.2. SOC Estimation by the SVSF

With parameters estimated by the FUDRLS algorithm, the SVSF can be employed to estimate the battery SOC based on the model (2). Originally proposed in [47] and built on integration of the variable structure theory and the sliding mode notion, the SVSF is a predictor-corrector method for state and parameter estimation. A schematic diagram of the SVSF-based state estimation is shown in Fig. 4, where the solid line is the system state trajectory. The estimated state trajectory is forced towards the system state trajectory until it enters a neighborhood of the actual state trajectory, referred to as the existence subspace. The existence subspace is an invariant set because once the estimated state enters, it remains within the region driven by a switching gain. The SVSF demonstrates good robustness to modeling uncertainties and noises, given that uncertainties are upper-bounded. It has been applied to estimate battery parameters and the SOC in [48], with only simulation results available.

3.2.1. The SVSF

The dynamics of the SVSF are given by

$$\begin{aligned} \hat{X}_{k+1|k} &= f(\hat{X}_{k|k}, i_B(k)), \\ \hat{y}_{k+1|k} &= C_{SVSF}\hat{X}_{k+1|k}, \end{aligned} \tag{11}$$

where $\hat{X}_{K+1|k}$ is the predicted state, $\hat{X}_{k|k}$ is the state estimate at time k, $\hat{y}_{k+1|k}$ is the predicted measurement, and C_{SVSF} is the linearized measurement matrix given by

$$C_{SVSF} = \frac{\partial h(X, i_B)}{\partial X} = \text{diag}\begin{bmatrix} \frac{\partial V_s(SOC)}{\partial SOC} & -1 & 1 \end{bmatrix}.$$

Defining the innovation as

$$e_{z,k+1|k} = y_{k+1} - C_{SVSF}\hat{X}_{k+1|k},$$

the SVSF gain is calculated as follows

$$K_{SVSF,k+1} = C_{SVSF}^{-1}(|e_{z,k+1|k}| + \gamma|e_{z,k|k}|) \circ \text{sat}(e_{z,k+1|k}, \Psi), \tag{12}$$

where $e_{z,k|k}$ is a posteriori measurement error; Ψ is the smoothing boundary layer widths; $\gamma \in (0,1)$ is the SVSF convergence rate; $\circ$ is the Schur product. To ensure the numerical stability, the components of C_{SVSF} should not take singular values. This can be accomplished by using a simple *if* statement with a very small threshold (i.e., 10^{-10}) or calculating the pseudoinverse C_{SVSF}^{-1} with a small damping parameter ω (e.g., 10^{-8}) as the following

$$C_{SVSF}^{-1} = C_{SVSF}^{T}(C_{SVSF}C_{SVSF}^{T} + \omega I_3)^{-1}. \tag{13}$$

The corrected (or posteriori) state estimates are computed as follows

$$\hat{X}_{k+1|k+1} = \hat{X}_{k+1|k} + K_{SVSF,k+1}.$$

3.3. SOH Estimation by the RTLS

As the maximum capacity is a key factor for the battery's health, this paper considers the following quantity as a measure of the SOH

$$SOH(n) = \frac{C_{\max}}{C_{\max new}}, \tag{14}$$

where n is the maximum capacity estimation algorithm update index, and $C_{\max new}$ is the maximum capacity of a new battery cell. Such an SOH represents the capacity degradation of the cell. Also, it is clear that an accurate $C_{\max}$ is prerequisite for Coulomb-counting-based SOC estimation algorithms to provide a good estimation of the SOC.

In [11, 49], the maximum capacity is simply calculated as follows

$$C_{\max} = \frac{T_s \Sigma_{k=k_1}^{k_2} \frac{\eta i_B(k)}{3600}}{SOC(k_2) - SOC(k_1)}, \tag{15}$$

where k_1 and k_2 are time indices. Rearrangement of (15) gives the following linear regression form

$$z = C_{\max} u,$$

where $u = SOC(k_2) - SOC(k_1)$ and

$$z = T_s \Sigma_{k=k_1}^{k_2} \frac{\eta i_B(k)}{3600}.$$

Under certain conditions on z and u, an unbiased estimation of $C_{\max}$ can be achieved by solving an LS problem. The total least squares (TLS) problem was proposed to alleviate the limitation of

the LS formulation by performing orthogonal regression [50].

The TLS problem is generally solved by using singular value decomposition (SVD) algorithms [50] which incur high computational complexity, and thus are not suitable for embedded applications [51]. In this paper, a fast RTLS algorithm is applied for maximum capacity estimation. The estimated maximum capacity will be consequently used for the SOH estimation using (14). The proposed RTLS algorithm is based on the constrained Rayleigh quotient, which can run in real time and enjoys fast convergence [52]. Compared to the TLS, the proposed RTLS algorithm entails much lower computational load, and the estimation accuracy is comparable to the TLS algorithm.

To facilitate the presentation of the proposed algorithm, it is firstly assumed that the noisy output and input are given by

$$\underbrace{z(n)-\Delta z}_{\tilde{z}(n)} = C_{\max}\underbrace{(u(n)-\Delta u)}_{\tilde{u}(n)}, \tag{16}$$

where $u(n)$ and $z(n)$ are the true input and output, respectively; $\tilde{u}_n$ and $\tilde{z}_n$ are the noisy input and output, respectively; the output error Δz is assumed zero-mean Gaussian with known variance of σ_z^2; the SOC estimation error Δu is assumed zero-mean Gaussian with known variance of σ_u^2. The autocorrelation matrix of the noisy input is defined as:

$$\tilde{R}_u(n) = E[\tilde{u}(n)\tilde{u}^T(n)] = R_u(n) + \sigma_u^2 I,$$

where $R_u(n) = E[u(n)u^T(n)]$. Define the augmented data $\bar{x}(n) = [\tilde{u}(n), \tilde{z}(n)]^T$. The autocorrelation matrix of $\bar{x}(n)$ can be expressed as

$$\bar{R}_x = E[\bar{x}(n)\bar{x}^T(n)] = \begin{bmatrix} R_u(n) & b(n) \\ b^T(n) & c(n) \end{bmatrix}$$

where $b(n) = E[\tilde{u}(n)\tilde{z}^T(n)]$ and $c(n) = E[\tilde{z}(n)\tilde{z}^T(n)]$. When n is sufficiently large, the stochastic quantities $R(n), b(n)$, and $c(n)$ can be expressed as follows [52]

$$\begin{aligned} R_u(n) &= \mu R_u(n-1) + \tilde{u}(n)\tilde{u}^T(n), \\ b(n) &= \mu b(n-1) + \tilde{u}(n)\tilde{y}^T(n), \\ c(n) &= \mu c(n-1) + \tilde{y}(n)\tilde{y}^T(n), \end{aligned}$$

where μ is the forgetting factor.

The maximum capacity estimation on the basis of (16) is performed by minimizing the following constrained Rayleigh quotient

$$J(C_{\max}) = \frac{q^T \bar{R}_x q}{q^T D q} = \frac{R_u C_{\max}^2 - 2bC_{\max} + c}{C_{\max}^2 + \beta} \tag{17}$$

where the eigenvector $q = [C_{\max}, -1]^T$, and $\bar{D} = \mathrm{diag}(1, \beta)$ is a diagonal matrix with $\beta = \sigma_z^2/\sigma_u^2$.

If the eigenvector vector q^* which minimizes $J(C_{\max})$ corresponds to the smallest eigenvalue of $\bar{R}_x$, then q^* is the unbiased TLS solution [53].

To avoid solving the constrained Rayleigh quotient minimization problem at each step, the $C_{\max}$ is assumed to be updated as follows

$$C_{\max}(n) = C_{\max}(n-1) + \alpha(n)\tilde{u}(n), \tag{18}$$

where $\alpha(n)$ is chosen to minimize (17) in the direction of $\tilde{u}(n)$, i.e.,

$$\frac{\partial J(C_{\max}(n-1) + \alpha(n)\tilde{u}(n))}{\partial \alpha(n)} = \frac{c_1\alpha^2(n) + c_2\alpha(n) + c_3}{d(\alpha(n))} = 0. \tag{19}$$

where

$$\begin{aligned}
c_1 &= 2\tilde{u}^3(n)b(n),\\
c_2 &= 2\tilde{u}^2(n)[2b(n)C_{\max}(n-1) + \beta R(n) - c(n)],\\
c_3 &= 2\tilde{u}(n)[b(n)C^2_{\max}(n-1) - (\beta R(n) + c(n))C_{\max}(n-1) + \beta b(n)].
\end{aligned}$$

Then, $\alpha(n)$ can be obtained by solving the following quadratic equation formed by the numerator term of (19):

$$c_1\alpha^2(n) + c_2\alpha(n) + c_3 = 0. \tag{20}$$

The quadratic equation (20) has two roots, from which the solution of $\alpha(n)$ can be obtained as follows

$$\alpha(n) = \frac{-c_2 + \sqrt{c_2^2 - 4c_1c_3}}{2c_1}. \tag{21}$$

4. Strategy Validation

Simulation and experiments are carried out to validate the proposed condition monitoring strategy for a Li-ion battery cell subject to various pulsed current operations. Comparisons with existing DEKF [20] methods demonstrate advantages of the proposed strategy in terms of estimation accuracy quantified by root mean square error (RMSE) and computational cost quantified by running time. Simulation and experiments are performed in MATLAB® on a computer with 2.2GHz Intel® Core™Duo 2 CPU T6600 and 64-bit OS.

4.1. Simulation Study: Non-Aging Case

For the non-aging case, simulation study assumes the battery model (2) with constant parameters and that the battery model is subject to a current profile which is proportional to the speed profile in the standard Urban Dynamometer Driving Schedule (UDDS). In an urban driving environment, a vehicle switches frequently between acceleration, deceleration and steady state. This would lead to battery discharging profiles containing sufficient frequencies, thus bringing about improved identifiability and observability of the battery model [19].

Table 2 lists the values of model parameters, which are based on a polymer Li-ion battery cell [37] but with the maximum capacity scaled up to 10 Ah. The initial actual and estimated states are set, respectively, as follows:

$$[SOC(0), V_d(0), V_h(0)]^T = [0.95, 0, 0]^T,$$
$$[\widehat{SOC}(0), \hat{V}_d(0), \hat{V}_h(0)]^T = [0.8, 0, 0]^T.$$

The initial maximum capacity $\hat{C}_{\max}$ of the estimators is set to be 6 Ah. The value of N_0 and δ_1 are defined as 50 and 0.995, respectively, for the FUDRLS with the proposed VF ($\lambda_{\min}$ = 0.95 and $\lambda_{\max}$ = 0.995). In the SVSF, the value of γ and Ψ are set to be 0.1 and 1. Input current is corrupted by zero-mean Gaussian noise with variance $\sigma_z^2 = (0.01)^2$. In the RTLS, the SOC estimation accuracy of the SVSF is assumed 1% (i.e., $\sigma_u = 0.01$), and thus an overall σ_u^2 is $2 \times (0.01)^2$ since two estimated SOC points are required [36]. Hence, $\beta = (0.001)^2/(0.01)^2$. Also, the forgetting factor $\mu = 0.98$. The DEKF [20], which includes an EKF for SOC estimation and another EKF for estimating R_s, R_c, C_d, and $C_{\max}$, is implemented to make comparison. In the DEKF design, the initial state covariance, process noise covariance matrix, and measurement noise covariance matrix, are defined as diag$[1,1,1]$, diag$[0.09, 0.09, 0.09]$ and 0.25, respectively; and those of the EKF for parameter estimation are specified as diag$[10^{-13}, 10^{-2}, 5\times10^{-2}, 10^{-4}]$, diag$[10^{-9}, 10^{-4}, 10^{-5}, 10^{-7}]$ and 0.25, respectively. The parameters of the proposed algorithms and the DEKF are selected by trial-and-error in an effort to minimize the estimation error.

Both the FUDRLS and the SVSF run at a sampling period $T_s = 1$ second, while the RTLS runs at a longer period $T_l = 200$ seconds. The DEKF however has only one sampling period: $T_s = 1$ second. Simulation results are shown in Fig. 5. Particularly, Fig. 5(a) plots the UDDS current profile; Fig. 5(b) gives the corresponding voltage response of the battery cell; Figs. 5(c)-5(e) compare the impedance estimation results; Fig. 5(f) shows the estimated SOC and the true SOC computed from the Coulomb counting; and Fig. 5(g) compares the estimated $C_{\max}$. One can see that the proposed algorithms lead to at least comparable estimation accuracy as the DEKF does. Table2 3-4 compare the proposed algorithms and the DEKF using performance metrics: RMSE as a measure of estimation accuracy and simulation time as a measure of computational load. Simulation shows that the proposed strategy outperforms the DEKF in the sense of comparable estimation accuracy but lower computational cost.

4.2. Simulation Study: Aging Case

Proceeding further, we make a more compelling simulation study to verify that the proposed condition monitoring algorithm detects effectively the aged cell condition. From Table 2, capacity fade and internal resistance deterioration are considered as major indicators in the aging battery cell, where the true $C_{\max}$ decreases from 15Ah to 12Ah and R_s increase linearly over time. Fig. 6 summarizes simulation results. Particularly, Fig. 6(a) gives the pulsed current cycle applied on the battery model; Fig. 6(b) shows the cell voltage; Fig. 6(c) compares the true R_s with its estimates; and Fig. 6(d) compares the true maximum capacity with its estimates. Simulation results indicate that the proposed method and the DEKF can track the R_s and the time-varying maximum capacity with similar accuracy.

4.3. Experimental Studies

The proposed condition monitoring algorithm is further validated against experimental data, which were collected from a $LiMn_2O_4$/hard-carbon battery in the Advanced Technology R&D Center, Mitsubishi Electric Corporation. The experiment was conducted, under the ambient temperature 21.6°, using a rechargeable battery test equipment produced by Fujitsu Telecom Networks. The tuning parameters of the proposed condition monitoring algorithm are given in Table 5. In the DEKF design, the initial state covariance, process noise covariance matrix, and measurement noise covariance matrix, used in the EKF for SOC estimation are defined as $\text{diag}[1,1,1]$, $\text{diag}[0.16,0.16,0.16]$ and 0.25, respectively; and those used in the EKF for parameter estimation are specified as $\text{diag}[10^{-14},10^{-4},10^{-5},10^{-6}]$, $\text{diag}[4\times10^{-10},10^{-7},10^{-10},10^{-11}]$ and 0.25, respectively. The true SOC trajectory is obtained using the Coulomb counting method. The parameters of the OCV-SOC function of the battery cell are extracted [40]. The estimated states $\hat{X}(0)$ and maximum capacity $\hat{C}_{\max}$ are initialized to be $[0.4,0,0]^T$ and 5 Ah, respectively; the true states $X(0)=[0.31,0,0]^T$ and $C_{\max}=4.732Ah$. In order to set the test battery cell with the desired initial SOC, the battery cell was first fully charged and rest for one hour. Then the cell is discharged using a small current (e.g., 0.2 A) to the desired initial SOC value. The true maximum capacity was extracted offline from full discharge test with a small current (e.g., 0.2 A) at ambient temperature before testing the battery.

At first, the FUDRLS is executed for 30 seconds to estimate parameters, and then the SVSF starts estimating the SOC. Both the FUDRLS and the SVSF have the same sampling period $T_s=1$ second, while the RTLS has a distinctive sampling period $T_l=20$ seconds. On the other hand, the DEKF runs at the sampling period $T_s=1$ second. Estimation results are shown in Fig. 7. Particularly, Fig. 7(a) shows the high pulse current cycle ($i_B=10$C) applied on the battery; Fig. 7(b) gives the measured cell voltage; Figs. 7(c)-7(e) show the impedance estimation results; Fig. 7(f) compares the estimated SOCs; and Fig. 7(g) compares the $C_{\max}$ estimates. One can observe: the proposed algorithms yield accurate SOC estimation; for the maximum capacity estimation, the proposed algorithms converge to the true value, albeit the DEKF does not; and the DEKF provides more consistent estimation of impedance parameters than the proposed algorithms. Table 6 summarizes simulation time and estimation accuracy of both condition monitoring algorithms. Experimental results validate that the proposed algorithms can provide reliable SOC and SOH estimation at fairly low computational cost, and thus can be suitable for real-time embedded BMSs for various applications.

5. Conclusions

Motivated to address the challenges arsing in the deployment and use of Li-ion batteries, this paper has proposed a novel model-based condition monitoring strategy for real-time impedance, SOC, and maximum capacity/SOH estimation. A set of interdependent algorithms have been constructed and validated by both simulation and experimental studies. Owing to its low complexity, easy implementation, and high accuracy, the proposed strategy will be particularly suitable for real-time embedded BMSs strongly demanded in applications such as EVs and PHEVs. In addition, the proposed strategy can be extended to build promising solutions to SOP and SOF estimation, battery prognosis and fault diagnosis. In the future work, the thermal and aging effects

will be incorporated, and adaptive condition monitoring will be investigated. Another future effort will be to develop capacity estimation approaches robust to colored noises, which will find important application in EVs and PHEVs.

References

[1] Y. Nishi, Lithium ion secondary batteries; past 10 years and the future, Journal of Power Sources 100 (1-2) (2001) 101–6.

[2] N. Chaturvedi, R. Klein, J. Christensen, J. Ahmed, A. Kojic, Algorithms for Advanced Battery-Management Systems, IEEE Control Systems Magazine 30 (3) (2010) 49–68.

[3] G. L. Plett, Extended Kalman filtering for battery management systems of LiPB-based HEV battery packs: Part 2. Modeling and identification, Journal of Power Sources 134 (2004) 262–76.

[4] L. Lu, X. Han, J. Li, J. Hua, M. Ouyang, A review on the key issues for lithium-ion battery management in electric vehicles, Journal of Power Sources 226 (2013) 272–88.

[5] L. W. Juang, P. J. Kollmeyer, R. D. Lorenz, Implementation of online battery state-of-power and state-of-function estimation in electric vehicle applications, in: Proc. IEEE Energy Conversion Congress and Exposition, 1819–26, 2012.

[6] G. L. Plett, Sigma-point Kalman filtering for battery management systems of LiPB-based HEV battery packs: Part 2: Simultaneous state and parameter estimation, Journal of Power Sources 161 (2) (2006) 1369–84.

[7] W. Gao, M. Jiang, Y. Hou, Research on PNGV model parameter identification of LiFePO4 Li-ion battery based on FMRLS, in: Proc. IEEE Industrial Electronics and Applications, 2294–7, 2011.

[8] M. A. Roscher, O. S. Bohlen, D. U. Sauer, Reliable state estimation of multicell lithium-ion battery systems, IEEE Transactions on Energy Conversion 26 (2011) 737–43.

[9] C. R. Gould, C. M. Bingham, D. A. Stone, P. Bentley, New battery model and state-of-health determination through subspace parameter estimation and state-observer techniques, IEEE Transactions on Vehicular Technology 58 (2009) 3905–16.

[10] H. R. Eichi, M. Chow, Adaptive parameter identification and state-of-charge estimation of lithium-ion batteries, in: Proc. 38th Annual Conference of the IEEE industrial Electronics Society, 3012–7, 2012.

[11] T. Kim, W. Qiao, L. Qu, Online SOC and SOH estimation for multicell lithium-ion batteries based on an adaptive hybrid battery model and sliding-mode observer, in: Proc. IEEE Energy Conversion Congress and Exposition, 292–8, 2013.

[12] X. Tang, X. Mao, J. Lin, B. Koch, Li-ion battery parameter estimation for state of charge, in: Proc. American Control Conference, 941–6, 2011.

[13] V. Pop, H. J. Bergveld, P. H. L. Notten, P. P. L. Regtien, State-of-the-art of battery state-of-charge determination, Measurement Science and Technology 16 (12) (2005) R93–110.

[14] W. X. Shen, K. T. Chau, C. C. Chan, Neural network-based residual capacity indicator for nickel-metal hydride batteries in electric vehicles, IEEE Transactions on Vehicular Technology 54 (2005) 1705–12.

[15] S. Malkhandi, Fuzzy logic-based learning system and estimation of state of charge of lead-acid battery, Engineering Applications of Artificial Intelligence 19 (2006) 479–85.

[16] T. Hansen, C. Wang, Support vector based battery state of charge estimator, Journal of Power Sources 141 (2005) 351–8.

[17] J. Lee, O. Nam, B. Cho, Li-ion battery SOC estimation method based on the reduced order extended Kalman filtering, Journal of Power Sources 174 (1) (2007) 9–15.

[18] A. Vasebi, S. M. T. Bathaee, M. Partovibakhsh, Predicting state of charge of lead-acid batteries for hybrid electric vehicles by extended Kalman filter, Energy Conversion Management 49 (2008) 75–82.

[19] H. Fang, Y. Wang, Z. Sahinoglu, T. Wada, S. Hara, State of charge estimation for lithium-ion batteries: An adaptive approach, Control Engineering Practice 25 (2014) 45–54.

[20] G. L. Plett, Extended Kalman filtering for battery management systems of LiPB-based HEV battery packs: Part 3. State and parameter estimation, Journal of Power Sources 134 (2) (2004) 277–92.

[21] M. A. Roscher, O. S. Bohlen, J. Vetter, OCV hysteresis in Li-ion batteries including two-phase transition materials, International Journal of Electrochemistry 2011.

[22] Y. Wang, H. Fang, Z. Sahinoglu, T. Wada, S. Hara, Nonlinear adaptive estimation of the state of charge for Lithium-ion batteries, in: Proc. IEEE Conference on Decision and Control, Florence, Italy, 4405–10, 2013.
[23] S. J. Moura, N. A. Chaturvedi, M. Krstic, Adaptive PDE observer for battery SOC/SOH estimation via an electrochemical model, ASME Journal of Dynamic Systems, Measurement, and Control .
[24] M. Charkhgard, M. Farrokhi, State of charge estimation for Lithium-ion batteries using neural networks and EKF, IEEE Transactions on Industrial Electronics 57 (2010) 4178–87.
[25] N. C. Moo, Y. Chen, Y. Hsieh, Enhanced coulomb counting method for estimating state-of-charge and state-of-health of lithium ion batteries, Applied Energy 86 (2009) 1506–11.
[26] F. Huet, A review of impedance measurements for determination of the state-of-charge or state-of-health of secondary batteries, Journal of Power Sources 70 (1998) 59–69.
[27] M. Coleman, W. G. Hurley, C. K. Lee, An improved battery characterization method using a two-pulse load test, IEEE Transactions on Energy Conversion 23 (2008) 708–13.
[28] J. Kim, B. H. Cho, State-of-charge estimation and state-of-health prediction of a Li-Ion degraded battery based on an EKF combined with a per-unit system, IEEE Transactions on Vehicular Technology 60 (2011) 4249–60.
[29] Z. Cheng, C. C. Mi, Y. Fu, J. Xu, X. Gong, Online battery state of health estimation based on genetic algorithm for electric and hybrid vehicle applications, Journal of Power Sources 240 (2013) 184–92.
[30] S. Samadani, R. Fraser, M. Fowler, A review study of methods for lithium-ion battery health monitoring and remaining life estimation in hybrid electric vehicles, SAE Technical Paper 2012-01-0125, 2012.
[31] A. A. Hussein, Capacity fade estimation in electric vehicles Li-ion batteries using artificial neural networks, in: Proc. IEEE Energy Conversion Congress and Exposition, 677–81, 2013.
[32] J. Liu, A. Saxena, K. Goebel, B. Saha, W. Wang, An adaptive recurrent neural network for remaining useful life prediction of lithium ion batteries, in: Proc. Annual Conference of the Prognostics and Health Management Society, 1–9, 2010.
[33] D. Andre, A. Nuhic, T. Soczka-Guth, D. U. Sauer, Comparative study of a structured neural network and an extended Kalman filter for state of health determination of lithium-ion batteries in hybrid electricvehicles, Engineering Applications of Artificial Intelligence 26 (2013) 951–61.
[34] C. Hu, B. D. Youn, J. Chung, A multiscale framework with extended kalman filter for lithium-ion battery SOC and capacity estimation, Applied Energy 92 (2011) 694–704.
[35] I. Kim, A technique for estimating the state of health of lithium batteries through a dual-sliding-mode observer, IEEE Transactions on Power Electronics 25 (2010) 1013–22.
[36] G. L. Plett, Recursive approximate weighted total least squares estimation of battery cell total capacity, Journal of Power Sources 196 (2011) 2319–31.
[37] T. Kim, W. Qiao, A hybrid battery model capable of capturing dynamic circuit characteristics and nonlinear capacity effects, IEEE Transactions on Energy Conversion 26 (2011) 1172–80.
[38] X. Hu, S. Li, H. Peng, A comparative study of equivalent circuit models for Li-ion batteries, Journal of Power Sources 198 (2012) 359–67.
[39] M. Verbrugge, E. Tate, Adaptive state of charge algorithm for nickel metal hydride batteries including hysteresis phenomena, Journal of Power Sources 126 (1-2) (2004) 236–49.
[40] G. Plett, Results of temperature-dependent LiPB cell modeling for HEV SOC estimation, in: Proc. the 21st Electric Vehicle Symposium, Monaco, 2005.
[41] T. Kim, Y. Wang, Z. Sahinoglu, T. Wada, S. Hara, W. Qiao, Fast UD factorization-based RLS online parameter identification for model-based condition monitoring of lithium-ion batteries, in: Proc. American Control Conference, Portland, OR, 4410–5, 2014.
[42] F. Huagen, Discrete-time signals and systems, Tech. Rep., TechTeach, http://techteach.no, 2005.
[43] J. M. Jover, T. Kailath, A parallel architecture for Kalman filter measurement update and parameter estimation, Automatica 22 (1986) 337–46.
[44] T. R. Fortescue, L. S. Kershenbaum, B. E. Ydstie, Implementation of self-tuning regulators with variable forgetting factors, Automatica 17 (1981) 831–5.
[45] bq2750x Datasheet, Theory and implementation of Impedance Track battery fuel-gausing algorithm, Texas Instrument, Dallas, TX, 2008.
[46] K. K. Parhi, VLSI Digital Signal Processling System: Design and Implementation, John Wiley & Sons, 2007.

[47] S. R. Habibi, The smooth variable structure filter, Proceedings of the IEEE 95 (2007) 1026–59.
[48] M. S. Farag, R. Ahmed, S. Gadsden, S. R. Habibi, J. Tjong, A comparative study of Li-ion battery models and nonlinear dual estimation strategies, in: Proc. IEEE Transportation Electrification Conference and Expo, 1–8, 2012.
[49] J. L. X. Tang, X. Mao, B. Koch, Capacity estimation for Li-ion batteries (2011) 947–52.
[50] I. Markovsky, S. V. Huffel, Overview of total least-squares methods, Signal Processing 87 (2007) 2283–302.
[51] K. Yang, J. An, X. Bu, G. Sun, Constrained total least-squares location algorithm using time-difference-of-arrival measurements, IEEE Transactions on Vehicular Technology 59 (2010) 1558–62.
[52] D. Z. Feng, X. D. Zhang, D. X. Chang, W. X. Zheng, A fast recursive total least squares algorithm for adaptive FIR Filtering, IEEE Transaction on Signal Processing 52 (2004) 2729–37.
[53] C. E. Davila, Efficient recursive total least squares algorithms for FIR adaptive filtering, IEEE Transaction on Signal Processing 42 (1994) 268–80.

List of Tables

List of Figures

1: algorithm initialization: set $k=0$, $\hat{\Theta}=\Theta_0$, and $P_0=\delta I_5=U_0D_0U_0^T$ where

$$U_0=\begin{bmatrix}1&0&0&0&\theta_1\\0&1&0&0&\theta_2\\0&0&1&0&\theta_3\\0&0&0&1&\theta_4\\0&0&0&0&-1\end{bmatrix},\quad D_0=\delta\begin{bmatrix}1&0&0&0&0\\0&1&0&0&0\\0&0&1&0&0\\0&0&0&1&0\\0&0&0&0&0\end{bmatrix}.$$

2: **repeat**
3: $k\leftarrow k+1$
4: read new data $V_B(k)$ and $i_B(k)$
5: compute $f=U_0^T\Phi_a(k)$
6: initialize $r(0)=\lambda$
7: **for** $h=1$ to 5 **do**
8: compute the parameters Gentleman's transformation

$$\begin{aligned}r(h)&=r(h-1)+D_0(h)f^2(h)\\D(h)&=D_0(h)r(h-1)/(\lambda r(h))\\\alpha(h)&=-f(h)\\\beta(h)&=D_0(h)f(h)/r(h)\\K(h)&=\beta(h)\end{aligned}$$

9: **end for**
10: **for** $j=2$ to 5 **do**
11: compute the Gentleman's transformation
12: **for** $i=1$ to $j-1$ **do**
13: compute the Gentleman's transformation

$$\begin{aligned}U(i,j)&=U_0(i,j)+\alpha(j)K(i)\\K(i)&=K(i)+\beta(j)U(i,j)\end{aligned}$$

14: **end for**
15: **end for**
16: update parameter estimate $\hat{\Theta}$ and U_0,D_0

$$\begin{aligned}\hat{\Theta}&=[U(1,5),U(2,5),U(3,5),U(4,5)]^T\\U_0&=U,\quad D_0=D\end{aligned}$$

17: map $\hat{\Theta}$ to $\hat{R}_s,\hat{R}_d,\hat{C}_d,\hat{b}_1$
18: check whether estimated parameters are within the predefined range of values
19: update the internal parameters
20: **until** parameter estimation task ends

Table 1: The FUDRLS algorithm.

Table 2: Simulated battery model parameters

$C_{\max}$	10Ah	C_d	4000F	R_s	0.06ohm	R_d	0.02ohm
$V_{h\max}$	0.01V	ρ	2.47e-4	a_0	-0.852	a_1	63.867
a_2	3.692	a_3	0.559	a_4	0.51	a_5	0.508

Table 3: Simulation comparison of RMSE for impedance estimation

	DEKF	FUDRLS
R_s (ohm)	7.4814e-4	2.9532e-4
R_c (ohm)	8.7396e-4	3.7908e-4
C_d (F)	359.85	178.06

Table 4: Simulation comparison of RMSE and simulation time

	FUDRLS	SVSF	RTLS	DEKF		
Estimation	Impedance	SOC	Capacity	Impedance	SOC	Capacity
Accuracy (RMSE)	In Table 3	0.0243	2.0989	In Table 3	0.0269	2.4685
Simulation Time (s)	0.8933	5.6676	0.0034	13.0559		

Table 5: Tuning parameters of the proposed algorithms

$\lambda_{\min}$	0.95	$\lambda_{\max}$	0.995	N_0	50
δ_1	0.995	γ	0.1	Ψ	1
υ	0.01	σ_u^2	$2(0.02)^2$	σ_z^2	$(0.01)^2$
μ	0.98	T_s	1	T_l	20

Table 6: Experimental comparison of RMSE and simulation time

	FUDRLS	SVSF	RTLS	DEKF		
Estimation	Impedance	SOC	Capacity	Impedance	SOC	Capacity
Accuracy (RMSE)	N/A	0.0171	0.1617	N/A	0.0220	0.2065
Simulation Time (s)	0.1474	0.9070	0.0061	2.0795		

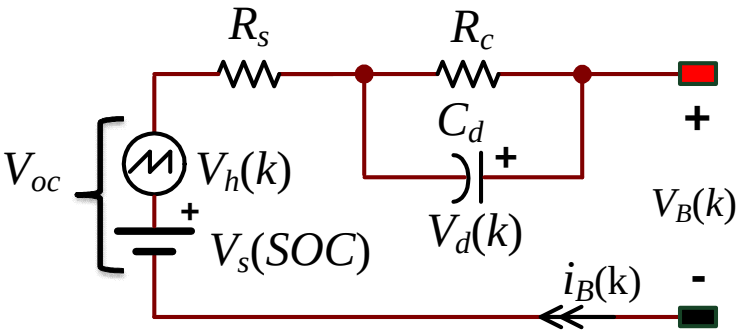

Figure 1: The first-order RC model with hysteresis

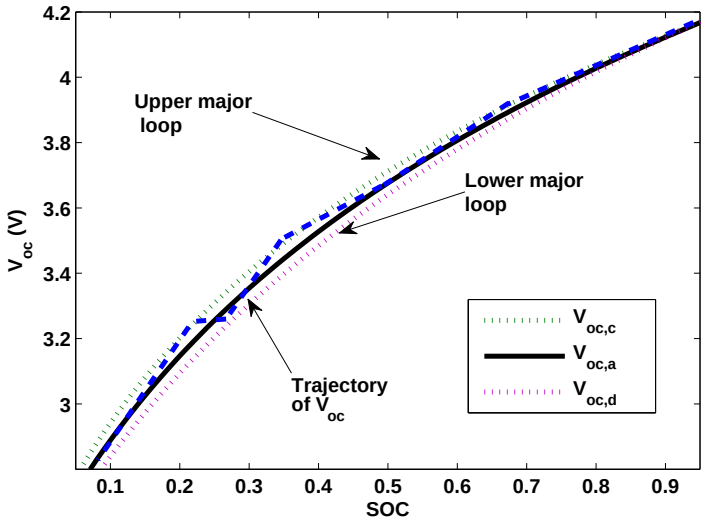

Figure 2: OCV-SOC curves

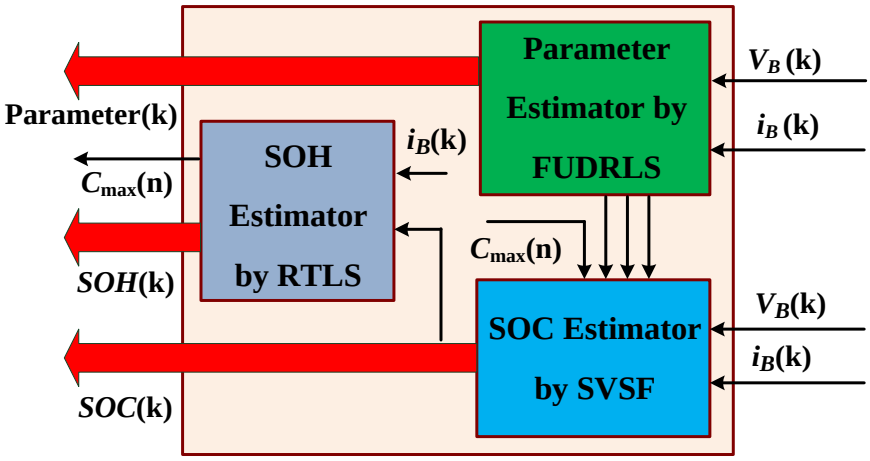

Figure 3: The proposed model-based condition monitoring method

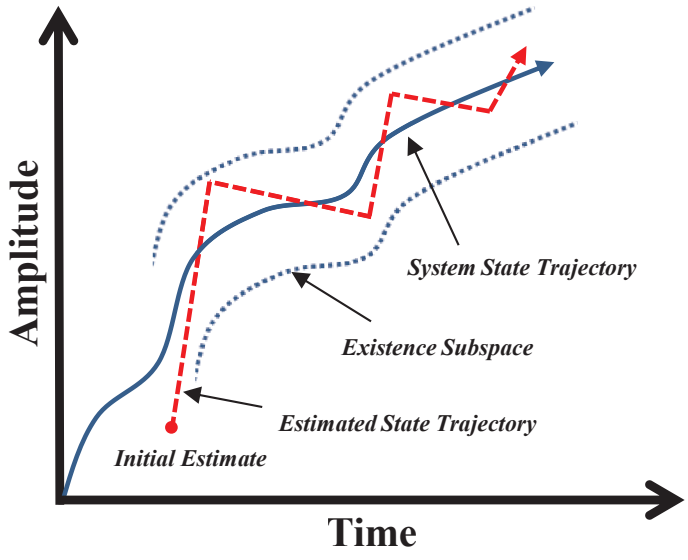

Figure 4: The SVSF estimation concept [47]

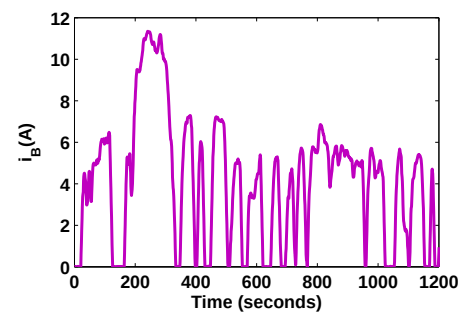

(a)

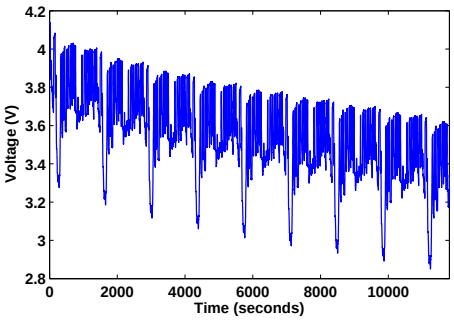

(b)

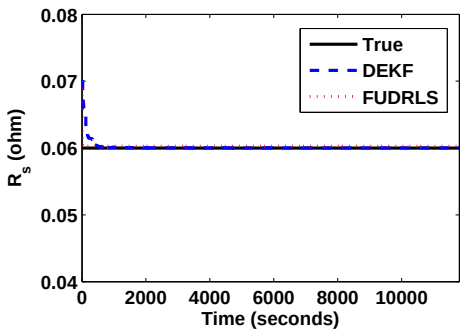

(c)

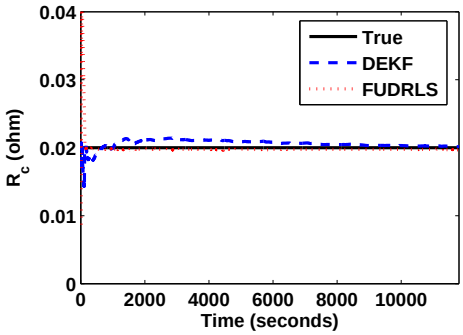

(d)

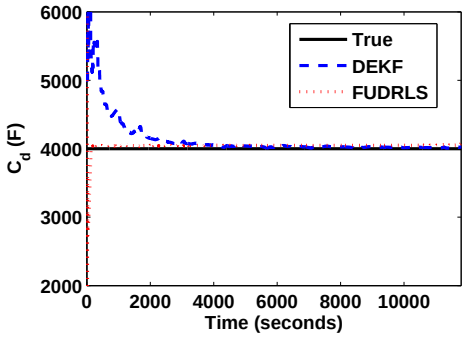

(e)

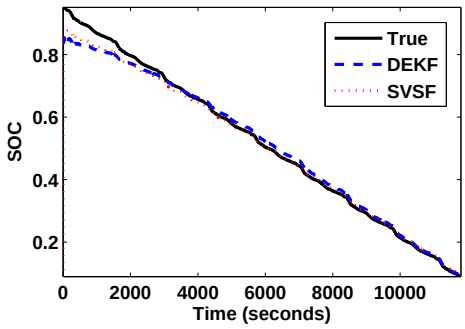

(f)

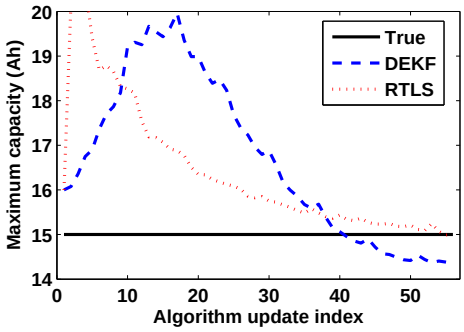

(g)

Figure 5: Comparison of true and estimated impedance, SOC, and maximum capacity of the battery model from the proposed condition monitoring algorithm and the DEKF: (a) input current profile; (b) cell voltage; (c) R_s and its estimates; (d) R_c and its estimates; (e) C_d and its estimates; (f) SOC and its estimates; and (g) $C_{\max}$ and its estimates.

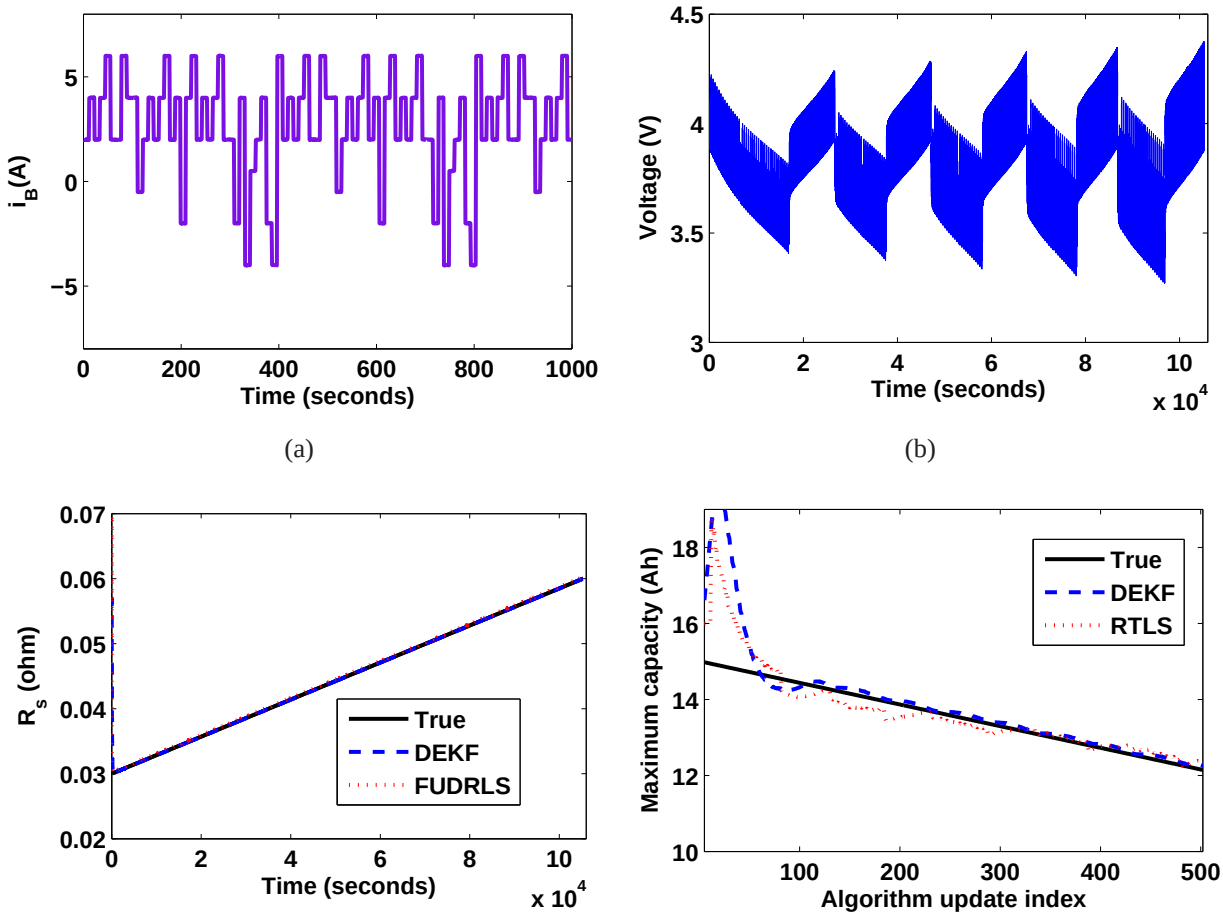

Figure 6: Comparison of true and estimated internal resistance and maximum capacity of the aged battery model from the proposed condition monitoring algorithm and the DEKF:(a) input current profile; (b) cell voltage; (c) R_s and its estimates; and (d) $C_{\max}$ and its estimates.

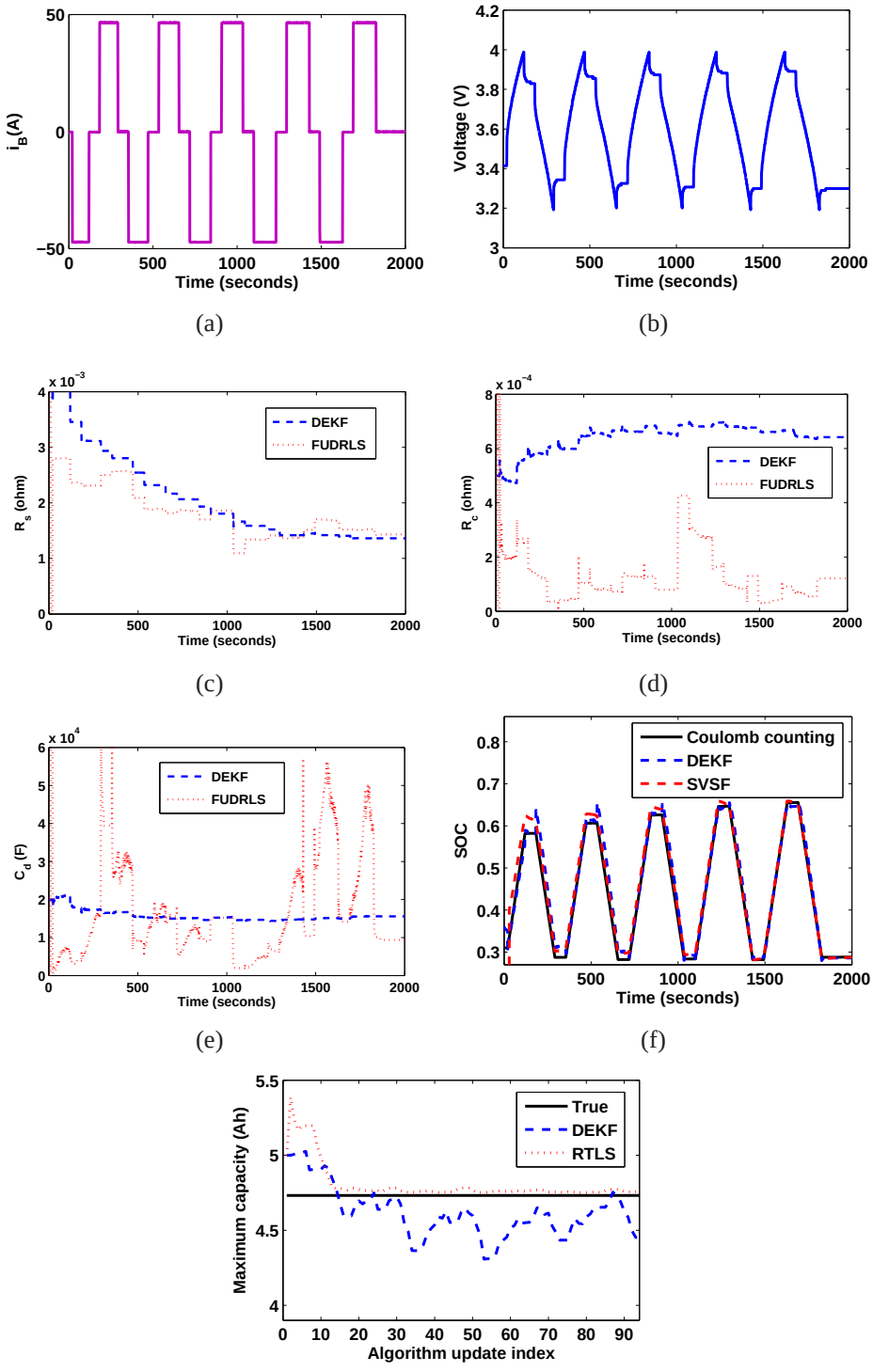

Figure 7: Estimated impedance, SOC, and maximum capacity from the proposed condition monitoring algorithm and a DEKF on the experimental data:(a) input current profile; (b) battery cell voltage response;(c) R_s estimates; (d) R_c estimates; (e) C_d estimates; (f) SOC and its estimates; and (g) $C_{\max}$ and its estimates.